







The Simultaneous Formation of Cored, Tangentially Biased, and Kinematically Decoupled Centers in Massive Early-type Galaxies

Antti Rantala¹ , Peter H. Johansson¹ , Thorsten Naab² , Jens Thomas³ , and Matteo Frigo²

¹Department of Physics, University of Helsinki, Gustaf Hällströmin katu 2, FI-00560 Helsinki, Finland; antti.rantala@helsinki.fi

²Max-Planck-Institut für Astrophysik, Karl-Schwarzschild-Str. 1, D-85748, Garching, Germany

³Max-Planck-Institut für Extraterrestrische Physik, Giessenbach-Str. 1, D-85741, Garching, Germany

Received 2018 December 6; revised 2019 February 4; accepted 2019 February 5; published 2019 February 14

Abstract

We study the impact of merging supermassive black holes (SMBHs) on the central regions of massive early-type galaxies (ETGs) using a series of merger simulations with varying mass ratios. The ETG models include realistic stellar and dark matter components and are evolved with the GADGET-3 based regularized tree code KETJU. We show that observed key properties of the nuclear stellar populations of massive ETGs, namely flat stellar density distributions (cores), tangentially biased velocity distributions, and kinematically decoupled (counter-)rotation, can naturally result from a single process—the scouring by SMBHs. Major mergers with mass ratios of $q > 1/3$ produce flat, tangentially biased cores with kinematically distinct components. These kinematic features originate from reversals of the SMBH orbits caused by gravitational torques after pericenter passages. Minor mergers ($q \lesssim 1/3$), on the other hand, form non-rotating cores and the orbit reversal becomes less important. Low-density stellar cores scoured in (multiple) minor mergers are less tangentially biased. This implies that the nuclear stellar properties of massive ETGs can be solely explained by stellar dynamical processes during their final assembly without any need for “feedback” from accreting black holes. We predict a strong correlation between decoupled cores, central anisotropy, and merger history: decoupled cores form in binary mergers and we predict them to occur in elliptical galaxies with the strongest central anisotropy. Measurements of the central orbital structure are the key to understanding the number of mergers that a given galaxy has experienced.

Key words: black hole physics – galaxies: elliptical and lenticular, cD – galaxies: kinematics and dynamics – methods: numerical

1. Introduction

The presence of supermassive black holes (SMBHs) is ubiquitous in all massive galaxies in the local universe (Kormendy & Ho 2013). A significant fraction of massive early-type galaxies (ETGs) show flat density profiles (Faber et al. 1997), tangentially biased central velocity dispersions (Thomas et al. 2014), and kinematic decoupling (e.g., Emsellem et al. 2007; Ene et al. 2018). In this Letter we present merger simulations of massive model ETGs with SMBHs and dark matter (DM) demonstrating that all three features, in quantitative agreement with observations, can result simultaneously from the merging of SMBHs in massive galaxies. In addition, this scouring process will not affect the homogeneity of the stellar population properties, such as their stellar ages and metallicities, in ETG centers.

Massive ETGs ($M_* \gtrsim 10^{10.8} M_\odot$) have photometric and stellar kinematic properties that differ from lower-mass ETGs (e.g., Kormendy et al. 2009). Their stellar components typically show slow or no global rotation (Emsellem et al. 2011). In addition, most massive ETGs have nearly flat central light profiles (cores) over a region that scales with the mass of the central black hole (BH; Lauer et al. 2007; Rusli et al. 2013) and its sphere of influence (Thomas et al. 2016). About $\sim 80\%$ of nearby massive and slowly rotating galaxies have cores (Krajnović et al. 2013) and the fraction of slow rotators rises rapidly with increasing stellar mass (Veale et al. 2017). Furthermore, detailed orbit models from the SINFONI BH survey revealed a very uniform orbital structure near the BH, with a predominance of tangential over radial motions (Thomas et al. 2014).

Theoretically the above features can be understood in a galaxy merger framework (Naab & Ostriker 2017). Massive ETGs are gas-poor systems and their late ($z < 2$) cosmological assembly is dominated by a phase of gas-poor (dry) merging, in which the ETGs accrete stars formed mainly in progenitors outside the main galaxy (e.g., De Lucia & Blaizot 2007; Oser et al. 2010; Johansson et al. 2012; Wellons et al. 2015; Rodriguez-Gomez et al. 2016). This provides plausible explanations for the observed rapid size growth (Naab et al. 2009), the high Sérsic indices of the surface brightness profiles (Hilz et al. 2013), and the slow rotation (Hernquist & Barnes 1991; Naab et al. 2014).

The formation of low-density cores and the observed velocity anisotropy can be explained by the scouring of stars in the centers by merging SMBHs (e.g., Milosavljević & Merritt 2001, 2003). Recent equal-mass merger simulations with more realistic multi-component ETG models, including SMBHs and DM halos, have shown that the cores become larger and the anisotropy is stronger for more massive BHs, which is in good agreement with observations (Rantala et al. 2018).

About half of the massive ETGs with cores show kinematic decoupling or counter rotation in their central region (Krajnović et al. 2013). In addition, the observed high stellar metallicities and old stellar ages are similar to the surrounding stellar populations (e.g., Bender et al. 1994). Galaxy merger simulations have long been able to explain the formation of counter-rotating cores (e.g., Barnes & Hernquist 1992). However, the process nearly always requires gas dissipation and counter-rotating retrograde merger orbits in order to produce

central kinematic decoupling (e.g., Balcells & Quinn 1990; Jesseit et al. 2007; Bois et al. 2011).

A recent study by Tsatsi et al. (2015) reported a kpc-scale counter-rotating old stellar component in a prograde simulation of merging gas-rich disks. They attributed this formation process to reactive forces during the merger that cause a short-lived change in the orbital spins of the progenitor galaxies. However, gas dissipation in galaxy centers and the resulting star formation results in even denser power-law density profiles and no cores (e.g., Barnes & Hernquist 1991; Hopkins et al. 2009). In addition, it seems difficult to construct a fine-tuned scenario where AGN feedback, acting at the right time, would allow for the formation of kinematically decoupled cores (KDCs) and still expel the gas to prevent the formation of a density cusps (e.g., Capelo & Dotti 2017; Frigo et al. 2018). A plausible scenario for the formation of tangentially biased and decoupled cores is therefore still missing.

In this Letter we present a dissipationless merger scenario that allows for the simultaneous formation of tangentially biased and KDCs with homogeneous stellar population properties.

2. Numerical Simulations

2.1. The KETJU Code

The simulations are run using the KETJU code (Rantala et al. 2017), an extension of the widely used tree-SPH simulation code GADGET-3 (Springel 2005). The key feature of the code is the inclusion of a regularized region around every SMBH in a simulation. The non-softened gravitational dynamics of systems of SMBHs and stars around any SMBH ($r < r_{\text{chain}}$) in the simulation is computed using the regularized AR-CHAIN (Mikkola & Merritt 2008) integrator, while the dynamics of the remaining particles is computed with the GADGET-3 leapfrog using the tree force calculation method (Rantala et al. 2017, 2018). The combination of the regularized integrator and GADGET-3 enables simulations with high particle numbers and accurate small-scale SMBH dynamics.

As in Rantala et al. (2018) we set $r_{\text{chain}} = 10$ pc for the size of the subsystems. The gravitational softening lengths are set to $\epsilon_{\text{DM}} = 100$ pc and $\epsilon_{\star} = 3.5$ pc for the DM and stellar particles, respectively. Particles within $r < r_{\text{pert}}$ of any SMBH act as near-field perturbers of the regularized subsystem, with $r_{\text{pert}} = 2 \times r_{\text{chain}}$, whereas the more distant particles act as far-field perturbers. The GADGET-3 integrator accuracy and the standard tree cell opening criterion parameter are set to $\eta = 0.002$ and $\alpha = 0.005$. We set the AR-CHAIN Gragg-Bulirsch-Stoer (GBS) tolerance to $\eta_{\text{GBS}} = 10^{-6}$. Post-Newtonian corrections up to order PN3.5 are used in the equations of motion of the SMBHs.

2.2. Initial Conditions

The progenitor galaxies consist of a Dehnen (1993) stellar component ($\gamma = 3/2$), a Hernquist ($\gamma = 1$) DM halo, and a central SMBH. The isotropic velocity profiles of the progenitors are constructed using the distribution function method and Eddington’s formula (Binney & Tremaine 2008). The parameters (M_{DM} , M_{\star} , M_{\bullet} , R_{e}) of the progenitor galaxies are presented in Table 1.

The most massive progenitor galaxy, IC-5, is identical to the IC “ γ -1.5-BH-6” of Rantala et al. (2018). The progenitors IC-1–IC-4 are scaled-down versions of IC-5, the masses of the components divided by a factor of 2–5. The effective radius of the least

massive progenitor IC-1 is smaller by a factor of two compared to the most massive progenitor (IC-5; Hilz et al. 2012); the progenitors IC-2, IC-3, and IC-4 have effective radii intermediate between these two values following a power-law scaling. The DM scale radius a_{DM} is chosen to set the DM fraction to $f_{\text{DM}} = 0.25$ within R_{e} (Rantala et al. 2018). The particle masses are $m_{\text{DM}} = 7.5 \times 10^6 M_{\odot}$ and $m_{\star} = 1.0 \times 10^5 M_{\odot}$.

For the base simulation we chose the γ -1.5-BH-6 run from Rantala et al. (2018) with a NGC 1600-like SMBH mass, which is somewhat above the host galaxy–BH scaling relations. We simulate five binary galaxy mergers including SMBHs with mass ratios of 1:1, 2:1, 3:1, 4:1, and 5:1 (merger remnants ETG-5-1 to ETG-1-1). The 1:1 merger is additionally run without SMBHs (ETG-1-1-nobh). We continue the 5:1 merger run with subsequent merger generations until five minor mergers are completed (ETG-M-B; Hilz et al. 2013). We remerge remnant ETG-1-1 with an identical remnant to study whether or not the physical features (core, anisotropy, rotation) formed in the first merger disappear in a second major merger (ETG-M-A). The eight merger remnants are listed in the middle and bottom panels of Table 1.

All merger orbits are nearly parabolic the pericenter distance being $r_{\text{p}} \sim 0.5 \times R_{\text{e}}$ of the host galaxy. After each minor merger, the merger remnant is reoriented so that the satellite galaxies fall in from random directions with respect to the principal axis of the host. All simulations were run until the gravitational-wave-driven final SMBH merger, with the maximum merger timescale being ~ 4 Gyr.

3. Results

3.1. Surface Brightness Profiles, Mass Deficits, and Velocity Anisotropies

The surface brightness profiles of the merger remnants ETG-1-1, ETG-1-1-nobh, ETG-M-A, and ETG-M-B are presented in Figure 1. The observed surface brightness profiles of three ellipticals with large cores (NGC 1600 and NGC 4472, NGC 5328) from Rusli et al. (2013) are shown for a qualitative comparison. Most simulated merger remnants have lower central surface brightness compared to the observed galaxies. We attribute this quantitative difference to the fact that our simulations contain very massive SMBH binaries, with masses well above the typical values inferred from the SMBH–host galaxy relation (Thomas et al. 2016; Rantala et al. 2018).

The final stellar and SMBH masses of the remnants ETG-1-1, ETG-1-1-nobh, and ETG-M-B are equal. We compute the central mass deficits from the surface brightness profiles in the core region ($r < r_{\text{b}}$) of the two merger remnants with SMBHs with respect to the non-scoured remnant ETG-1-1-nobh. Repeated minor mergers (ETG-M-B) result in a higher mass deficits. In five consecutive minor mergers, the $M_{\text{def}}/M_{\bullet}$ increases as $M_{\text{def}}/M_{\bullet} = 0.58$ (0.50), 1.55 (1.00), 2.46 (1.50), 3.08 (2.00), 3.45 (2.50). The values in the parenthesis are estimates by Merritt (2006): $M_{\text{def}}/M_{\bullet} \sim 0.5\mathcal{N}$, in which \mathcal{N} is the number of mergers. Our somewhat higher mass deficits are explained by the fact that Merritt (2006) measures the deficits when the binaries become hard, whereas we follow the binary evolution to smaller separations.

The velocity anisotropy profiles, $\beta(r) = 1 - \sigma_{\text{t}}^2/2\sigma_{\text{r}}^2$, of the four simulated mergers remnants are shown in Figure 1 with three observed galaxies (Thomas et al. 2014; Saglia et al. 2016). The profiles are computed in radial bins with a bin width

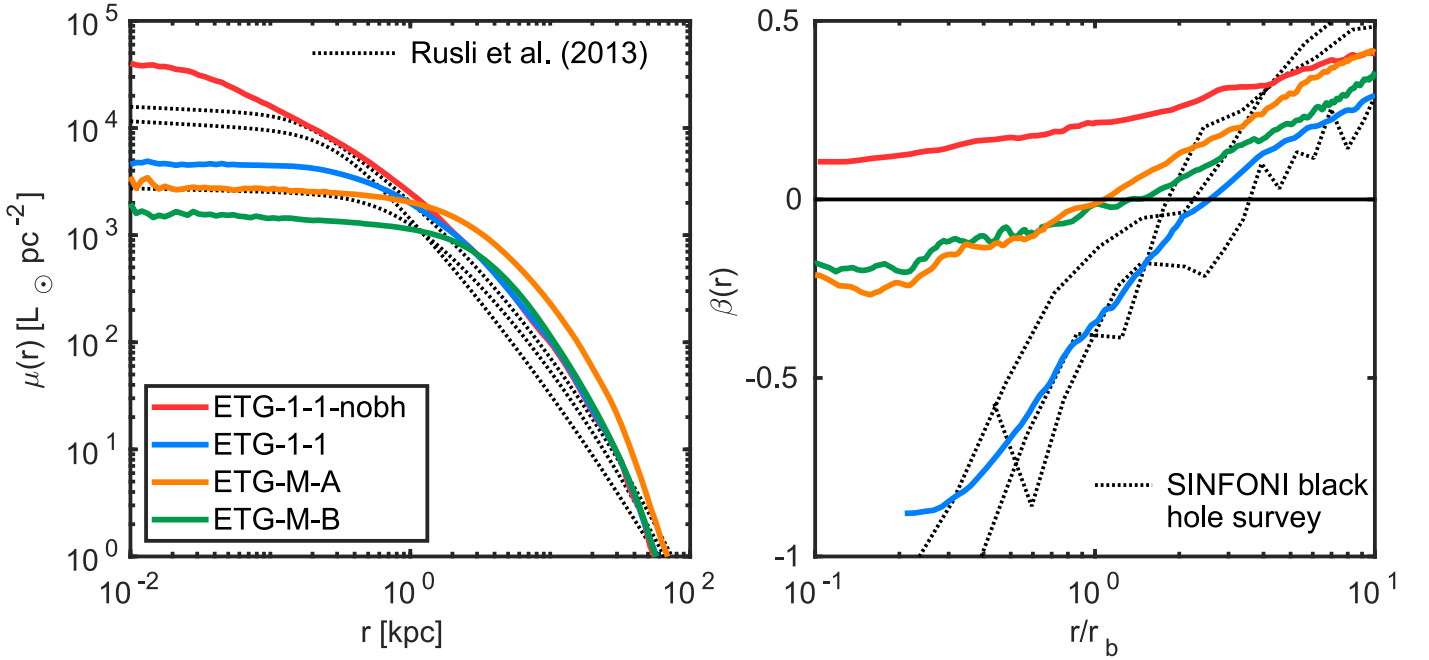


Figure 1. Left panel: the surface brightness profiles $\mu(r)$ of four representative merger remnants, $M/L_{\star} = 4.0$ (Thomas et al. 2016). Observed surface brightness profiles from Rusli et al. (2013) are shown as dotted lines. The core-Sérsic fits yield core radii of $r_b = 0.49$ kpc (ETG-1-1), $r_b = 1.51$ kpc (ETG-M-A), and $r_b = 1.55$ kpc (ETG-M-B), respectively. Right panel: the stellar velocity anisotropy profiles of the remnants with observed profiles of core ellipticals (dashed black lines; Saglia et al. 2016). For the run without SMBHs (red line) we set $r_b = 1$ kpc. Binary major mergers without SMBHs yield radially biased anisotropy profiles, while the inclusion of the SMBHs (blue line) produces a strongly tangentially biased velocity distribution in the core region. Repeated mergers (green and orange lines) render the central velocity distribution closer to isotropic.

Table 1
The Properties of the Progenitor Galaxies and Merger Remnants in this Study

Initial Conditions						
Progenitor	$M_{\text{DM}} [10^{13} M_{\odot}]$	$M_{\star} [10^{10} M_{\odot}]$	$M_{\bullet} [10^9 M_{\odot}]$	R_c [kpc]	$N_{\text{DM}} [\times 10^6]$	$N_{\star} [\times 10^6]$
IC-1	1.50	8.30	1.70	3.50	2.00	0.83
IC-2	1.88	10.34	2.13	4.16	2.50	1.04
IC-3	2.50	13.83	2.93	4.95	3.33	1.38
IC-4	3.75	20.75	4.25	5.90	5.00	2.08
IC-5	7.50	41.50	8.50	7.00	10.00	4.15
IC-5-nobh	7.50	41.50	...	7.00	10.00	4.15
Binary Mergers						
Merger remnant	$M_{\text{DM}} [10^{13} M_{\odot}]$	$M_{\star} [10^{10} M_{\odot}]$	$M_{\bullet} [10^9 M_{\odot}]$	Merged progenitors	Mass ratio	
ETG-5-1	9.00	49.80	10.20	IC-5 + IC-1	5:1	
ETG-4-1	9.38	51.88	10.63	IC-5 + IC-2	4:1	
ETG-3-1	10.00	55.33	11.33	IC-5 + IC-3	3:1	
ETG-2-1	11.25	62.25	12.75	IC-5 + IC-4	2:1	
ETG-1-1	15.00	83.00	17.00	IC-5 + IC-5	1:1	
ETG-1-1-nobh	15.00	83.00	...	IC-5-nobh + IC-5-nobh	1:1	
Multiple Merger Generations						
Merger remnant	$M_{\text{DM}} [10^{13} M_{\odot}]$	$M_{\star} [10^{10} M_{\odot}]$	$M_{\bullet} [10^9 M_{\odot}]$	Merged progenitors	Mass ratio	
ETG-M-A	30.00	166.00	34.00	ETG-1-1 + ETG-1-1	1:1	
ETG-M-B	15.00	83.00	17.00	IC-5 + 5 × IC-1	5:1–9:1	

of 0.2 kpc. The anisotropy profile of ETG-1-1-nobh is radially biased ($\beta > 0$) in the absence of SMBH binary. As in Rantala et al. (2018), the remnant ETG-1-1 is strongly tangentially biased ($\beta < 0$) in the core region, being in good agreement with the velocity anisotropy profiles of the observed core galaxies. The repeated mergers produce remnants ETG-M-A and ETG-M-B, which are mildly tangentially biased in the

central region, with each merger generation rendering the velocity anisotropy profile of the core region closer to isotropic.

The core sizes of the merger remnants built up in multiple mergers are $r_b \sim 1.5$ kpc, measured using the core-Sérsic fit (Graham et al. 2003). This is in contrast to the cores formed in a single binary merger for which we find $r_b \lesssim 0.5$ kpc. As the SMBH of the simulated remnant ETG-1-1 ($r_b \sim 0.5$ kpc) is at the

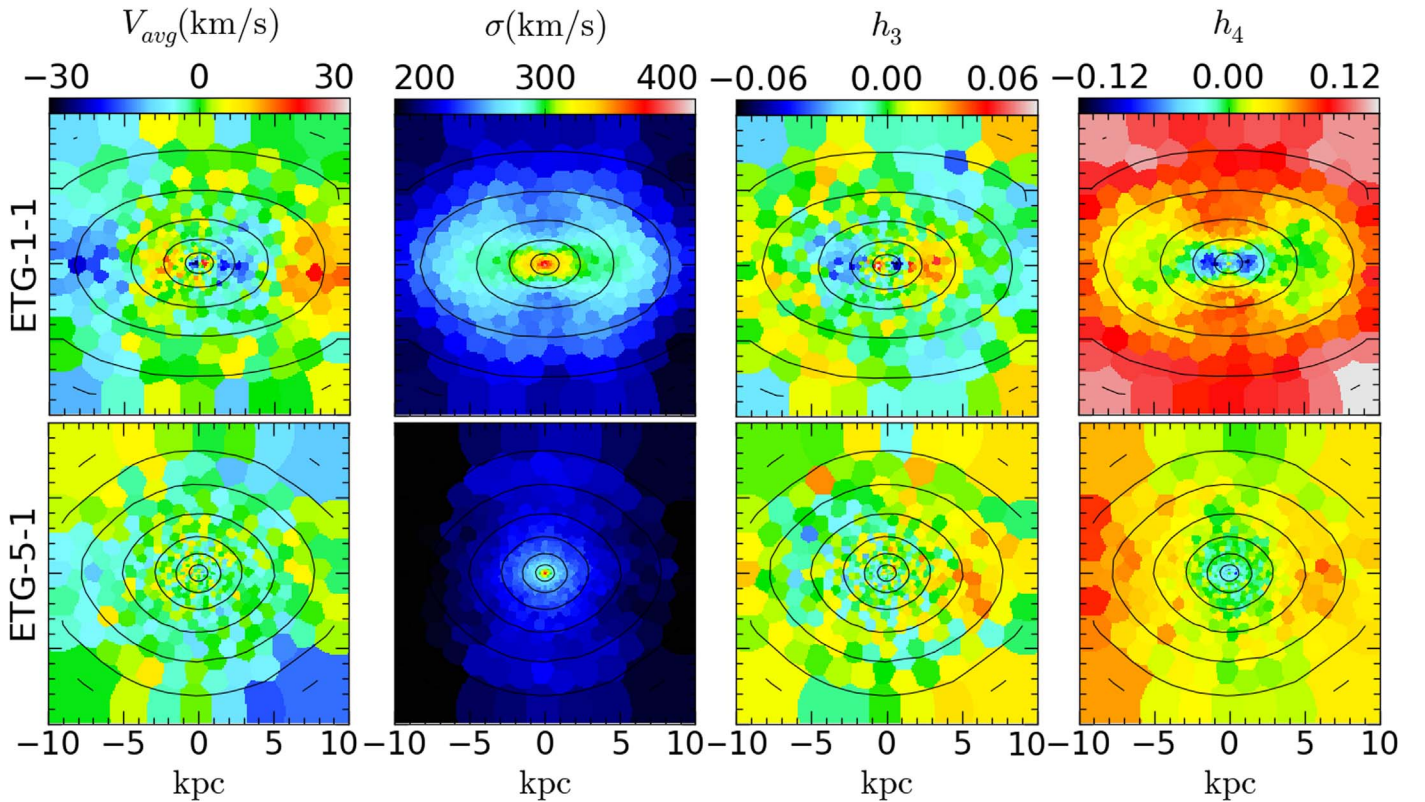


Figure 2. 2D kinematic maps of the merger remnants ETG-1-1 (top row) and ETG-5-1 (bottom row) presenting the mean LOS velocity, velocity dispersion, and Gauss–Hermite moments h_3 and h_4 . The binary major merger remnant ETG-1-1 shows complex central rotation signatures with an anticorrelation of V_{avg} and h_3 . The minor merger remnant ETG-5-1 does not show such rotation features.

upper end of the observed SMBH masses, $M_* = 1.7 \times 10^{10} M_\odot$, it seems probable that very large cores ($r_b \sim 3\text{--}4$ kpc) are formed more gradually by a large number of minor mergers with SMBHs (Merritt 2006).

Simulations focusing on SMBH binaries in isolated galaxies or equal-mass binary mergers have connected flat low-density stellar cores in ETGs to central tangentially biased velocity anisotropies (Quinlan & Hernquist 1997; Milosavljević & Merritt 2001; Rantala et al. 2018). Our results demonstrate that the formation of a stellar core by SMBH binary scouring produces a significantly less tangentially biased orbit distribution if the core was formed in a series of minor mergers instead of a single major merger. For individual galaxies, orbit modeling is the key to understanding their orbital structure and merger history (Thomas et al. 2014). Decoupled kinematic features are projection dependent and will only be observable at appropriate viewing angles.

3.2. Stellar Kinematics

Figure 2 presents the 2D kinematic maps of the merger remnants ETG-1-1 and ETG-5-1. The 2D maps are divided into Voronoi spaxels with an equal signal-to-noise ratio in each spaxel (Cappellari & Copin 2003; Naab et al. 2014). The V_{avg} , σ , h_3 , and h_4 are computed in each spaxel by fitting a Gauss–Hermite function to the histogram of line-of-sight (LOS) velocities (van der Marel & Franx 1993). The galaxies are oriented using the reduced inertia tensor, the major axis lying on the x -axis of the panels. The surface brightness data is overlaid as black contour lines with a spacing of 1 mag. We present the mean LOS velocity maps of all eight simulated merger remnants in Figure 3.

We characterize the rotation of the merger remnants using the spin parameter–ellipticity (ϵ , λ_R) criterion of Emsellem et al. (2011). We find that the spin parameter is small for every remnant, $\lambda_R < 0.03$, while the ellipticities are moderate, typically in the range $0.4 < \epsilon < 0.5$. All of our simulated merger remnants are slow rotators.

Decoupled rotation is seen in remnants ETG-1-1, ETG-2-1, and ETG-M-A, all harboring SMBH binaries with mass ratios of $q = M_2/M_1 \gtrsim 0.5$. In particular, the major merger remnant ETG-1-1 shows multiple decoupled rotating kinematic subsystems, indicated by the anticorrelation of V_{avg} and h_3 (e.g., Bender et al. 1994). The maximum rotation velocity is $\sim 30\text{--}40$ km s $^{-1}$. The mean velocity maps of minor merger remnants formed in ETGs 3-1, 4-1, 5-1, and M-B either show slow rotation at >5 kpc or are completely featureless. The remnant ETG-1-1-nobh shows clear rotation 5–10 kpc from the center, while the central region itself is non-rotating.

We use the kinemetry method of Krajnović et al. (2011) to analyze the rotation features of the merger remnants. All of our merger remnants are non-regular rotators (NRR) as deviations from simple rotation are significant. Using the kinematic types of Krajnović et al. (2011) we classify ETG-4-1, ETG-5-1, and ETG-M-B as type NRR-low rotation velocity (NRR-LV; <5 km s $^{-1}$). ETG-1, ETG-2, and ETG-M-A harbor counter-rotating cores (CRCs). The classification of ETG-3-1 and ETG-1-1-nobh is somewhat spurious as the outer parts of the galaxies are rotating while the core regions are not.

3.3. Origin of the Rotation Features in Core Ellipticals

In Figure 4 we show the origin of the complex rotation features of the major merger remnant ETG-1-1. In this

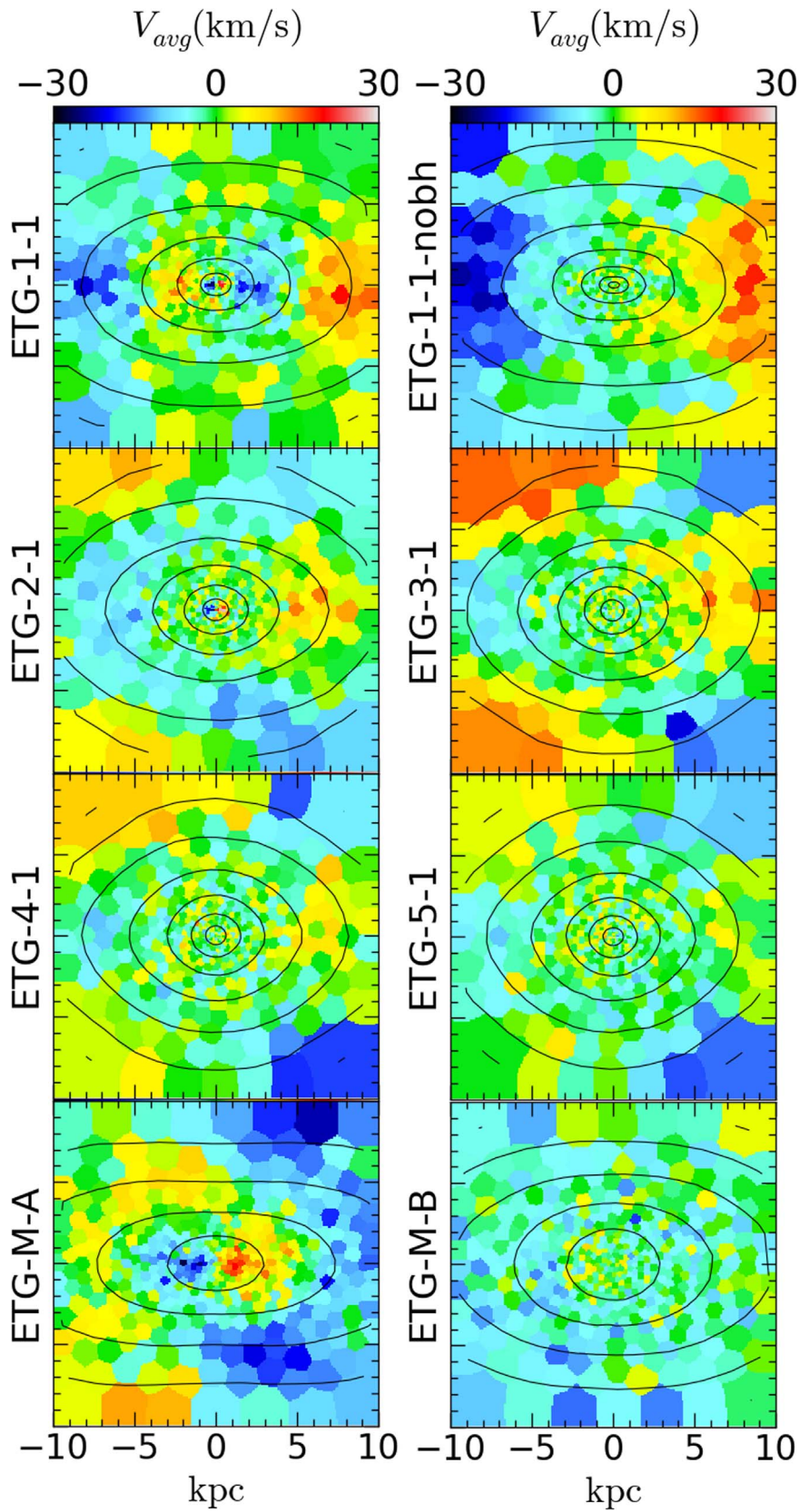


Figure 3. 2D kinematic maps of average LOS velocities of the merger remnants. Binary major mergers with SMBHs produce complex, decoupled kinematic regions at the central region. These features are weak or absent in minor mergers with SMBHs and in simulations without SMBHs.

simulation, the relative angular momentum of the SMBHs changes its sign three times during the galaxy merger. We relate the orbit reversals to two physical processes. Barnes (2016)

described a major merger process in which two bulges have a close encounter and are deflected from the major axis connecting their dark halos. The resulting gravitational torque reverses the

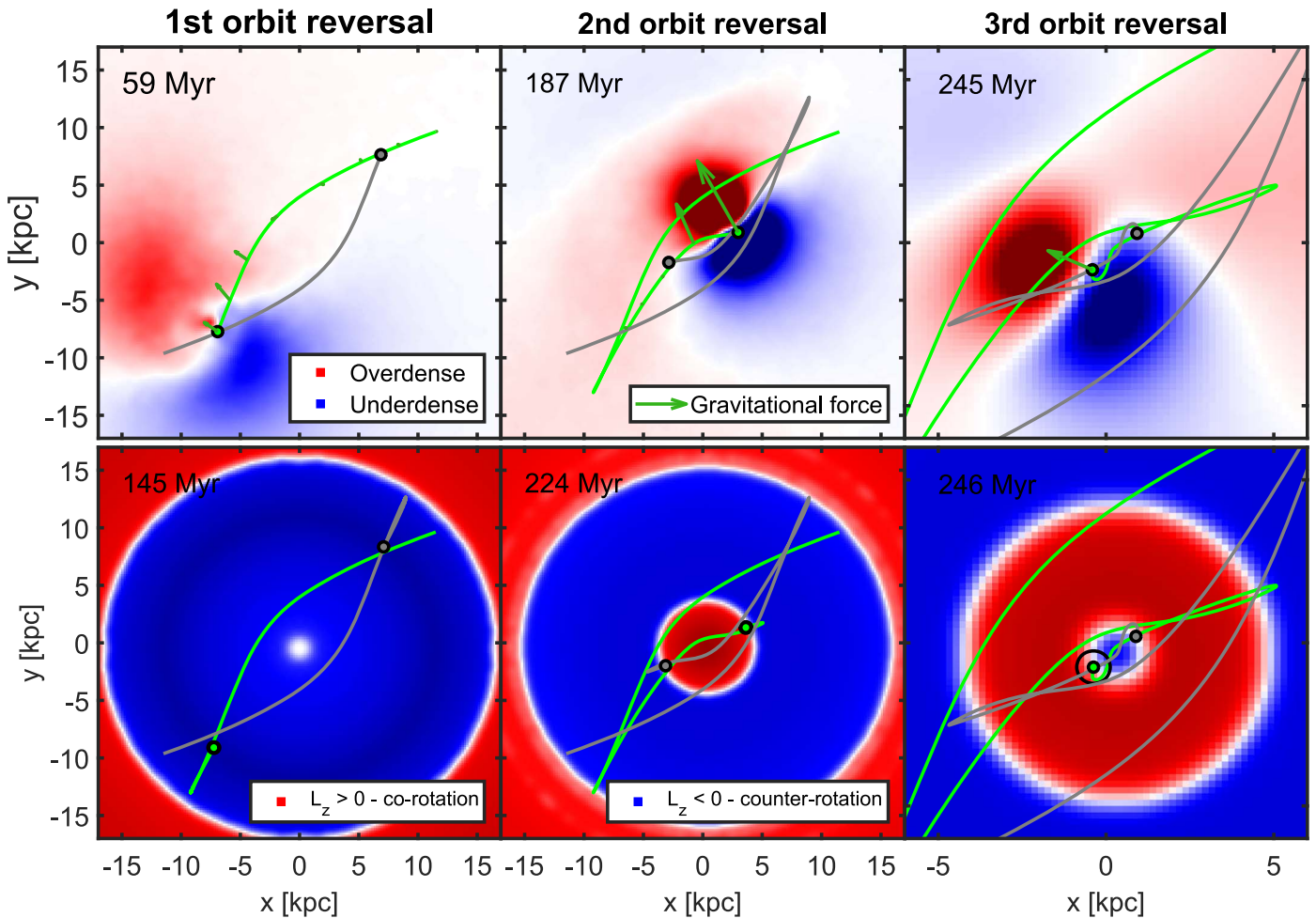


Figure 4. Top panels: the reversals of the merger orbit in the run ETG-1-1. The panels show the SMBH orbits (green and gray), the stellar overdense and underdense regions (single progenitor), and the gravitational force vector from the tidal debris on one of the SMBHs. The vector is scaled down by a factor of 10 smaller in the right panel. Bottom panels: the azimuthally averaged stellar rotation direction (both progenitors). The apocenter distances determine where the average stellar rotation direction changes sign. The influence radius r_{infl} of a single SMBH is marked with a black circle in the bottom panels, but is visible only in the right zoom-in panel as in the other panels it is smaller than the SMBH symbol.

relative angular momentum of the bulges. Another important effect is “tidal self-friction” described in van den Bosch & Ogiya (2018), in which the center of the subhalo is strongly pulled to the direction of the tidally expelled material, resulting in the reversal of the orbit.

The angular momentum reversals occur after the pericenter passages of the galaxies, before the apocenter. The encounter expels tidal debris from the galaxies, which pulls the centers of the galaxies to the direction of the stellar overdensity. Both dark matter and stars are important in the first orbit reversal, but later the effect of DM becomes negligible. The apocenter distances of the progenitors after each flip correspond to the locations where the stellar angular momentum and the mean LOS velocity in the kinematic maps change their signs. This connects the large-scale merger orbits to the complex velocity features observed in the LOS velocity distribution maps.

We performed tests in which the other galaxy was replaced by a static potential, and the orbit reversals occurred in these simulations as well. We also varied the pericenter distance by factors of 0.5–2 and the initial velocity by a factor of two. Each of these merger orbits had at least one orbit reversal. However, we stress that a more detailed study of the progenitor and merger orbit parameters is still required in order to assess how

generic orbital reversals are in these types of merger simulations.

In Figure 3 the outer rotation features are only seen in binary major mergers. Rantala et al. (2018) showed that a more centrally concentrated initial stellar density profile produces more strongly rotating outer regions, and that the central decoupled region becomes more prominent with increasing initial SMBH mass. Comparing the velocity maps of ETG-1-1, ETG-1-1-nobh, ETG-2-1, and ETG-3-1, the formation of the innermost decoupled region requires the presence of a close to equal-mass SMBH binary.

For less concentrated progenitor galaxies, smaller SMBH masses and large merger mass ratios the rotation features are weak or short-lived. Our simulations demonstrate that the binary mass ratios larger than approximately $q \gtrsim 1/3$ are needed to form long-lived central, kinematically decoupled regions in dry mergers of massive ETGs.

4. Conclusions

The binary major galaxy mergers presented in this study allow for the simultaneous formation of tangentially biased and kinematically distinct low-density cores in massive ETGs. Earlier formation models of these objects have relied on

dissipational effects or on the merger of rotating disk galaxies on prograde orbits in order to produce kinematically distinct central regions. However, forming an anisotropic low-density core with kinematically decoupled regions has proven difficult in these formation scenarios. Our progenitor galaxies are gas-free and initially non-rotating. Central kinematically distinct regions originate from the orbit reversals during the galaxy mergers.

The orbit reversals leave an imprint on the LOS velocity distributions of the merger remnants in the case of binary major mergers with mass ratios of $q \gtrsim 1/3$. Cuspy initial stellar profiles and more massive SMBHs lead to stronger central rotation signatures. The locations of the rotation reversals in the 2D kinematic maps correspond to the apocenters of the merger orbits after each orbit reversal (see Tsatsi et al. 2015). We also predict that, on average, galaxies with KDCs have a stronger central tangential anisotropy than galaxies without core rotation.

We find complex kinematic features in our cored merger remnants with mean LOS velocities in the range of $10\text{--}40 \text{ km s}^{-1}$ on spatial scales of up to ~ 20 core radii. These features are projection dependent, but our results demonstrate the feasibility of using rotation features as a first-order statistical tool to constrain the formation histories of massive, slowly rotating cored ETGs.

Finally, we have demonstrated that the formation of a low-density, flat central core in an ETG by SMBH binary scouring produces less tangential orbit anisotropy near the center if the core was scoured in a series of minor mergers with SMBHs. Our results stress that precise measurements of BH masses and of the central orbital structure, e.g., through Schwarzschild orbit superposition models, is the key to understanding the merger history of ETGs and their SMBHs.

The authors thank Simon White and Frank van den Bosch for discussions and valuable input. The numerical simulations were performed on facilities hosted by the CSC -IT Center for Science in Espoo, Finland. A.R. acknowledges support from the MPA Garching Visitor Programme. P.H.J. and A.R. acknowledge the support of the Academy of Finland grant 274931. T.N. acknowledges support from the DFG Cluster of Excellence “Origin and Structure of the Universe.”

ORCID iDs

Antti Rantala  <https://orcid.org/0000-0001-8789-2571>
 Peter H. Johansson  <https://orcid.org/0000-0001-8741-8263>
 Thorsten Naab  <https://orcid.org/0000-0002-7314-2558>
 Jens Thomas  <https://orcid.org/0000-0003-2868-9244>

References

- Balcells, M., & Quinn, P. J. 1990, *ApJ*, 361, 381
 Barnes, J. E. 2016, *MNRAS*, 455, 1957
 Barnes, J. E., & Hernquist, L. 1992, *ARA&A*, 30, 705
 Barnes, J. E., & Hernquist, L. E. 1991, *ApJL*, 370, L65
 Bender, R., Saglia, R. P., & Gerhard, O. E. 1994, *MNRAS*, 269, 785
 Binney, J., & Tremaine, S. 2008, *Galactic Dynamics* (2nd ed.; Princeton, NJ: Princeton Univ. Press)
 Bois, M., Emsellem, E., Bournaud, F., et al. 2011, *MNRAS*, 416, 1654
 Capelo, P. R., & Dottì, M. 2017, *MNRAS*, 465, 2643
 Cappellari, M., & Copin, Y. 2003, *MNRAS*, 342, 345
 Dehnen, W. 1993, *MNRAS*, 265, 250
 De Lucia, G., & Blaizot, J. 2007, *MNRAS*, 375, 2
 Emsellem, E., Cappellari, M., Krajnović, D., et al. 2007, *MNRAS*, 379, 401
 Emsellem, E., Cappellari, M., Krajnović, D., et al. 2011, *MNRAS*, 414, 888
 Ene, I., Ma, C.-P., Veale, M., et al. 2018, *MNRAS*, 479, 2810
 Faber, S. M., Tremaine, S., Ajhar, E. A., et al. 1997, *AJ*, 114, 1771
 Frigo, M., Naab, T., Hirschmann, M., et al. 2018, arXiv:1811.11059
 Graham, A. W., Erwin, P., Trujillo, I., & Asensio Ramos, A. 2003, *AJ*, 125, 2951
 Hernquist, L., & Barnes, J. E. 1991, *Natur*, 354, 210
 Hilz, M., Naab, T., Ostriker, J. P., et al. 2012, *MNRAS*, 425, 3119
 Hilz, M., Naab, T., & Ostriker, J. P. 2013, *MNRAS*, 429, 2924
 Hopkins, P. F., Cox, T. J., Dutta, S. N., et al. 2009, *ApJS*, 181, 135
 Jesseit, R., Naab, T., Peletier, R. F., & Burkert, A. 2007, *MNRAS*, 376, 997
 Johansson, P. H., Naab, T., & Ostriker, J. P. 2012, *ApJ*, 754, 115
 Kormendy, J., Fisher, D. B., Comell, M. E., & Bender, R. 2009, *ApJS*, 182, 216
 Kormendy, J., & Ho, L. C. 2013, *ARA&A*, 51, 511
 Krajnović, D., Emsellem, E., Cappellari, M., et al. 2011, *MNRAS*, 414, 2923
 Krajnović, D., Karick, A. M., Davies, R. L., et al. 2013, *MNRAS*, 433, 2812
 Lauer, T. R., Faber, S. M., Richstone, D., et al. 2007, *ApJ*, 662, 808
 Merritt, D. 2006, *ApJ*, 648, 976
 Mikkola, S., & Merritt, D. 2008, *AJ*, 135, 2398
 Milosavljević, M., & Merritt, D. 2001, *ApJ*, 563, 34
 Milosavljević, M., & Merritt, D. 2003, *ApJ*, 596, 860
 Naab, T., Johansson, P. H., & Ostriker, J. P. 2009, *ApJL*, 699, L178
 Naab, T., Oser, L., Emsellem, E., et al. 2014, *MNRAS*, 444, 3357
 Naab, T., & Ostriker, J. P. 2017, *ARA&A*, 55, 59
 Oser, L., Ostriker, J. P., Naab, T., Johansson, P. H., & Burkert, A. 2010, *ApJ*, 725, 2312
 Quinlan, G. D., & Hernquist, L. 1997, *NewA*, 2, 533
 Rantala, A., Johansson, P. H., Naab, T., Thomas, J., & Frigo, M. 2018, *ApJ*, 864, 113
 Rantala, A., Pihajoki, P., Johansson, P. H., et al. 2017, *ApJ*, 840, 53
 Rodriguez-Gomez, V., Pillepich, A., Sales, L. V., et al. 2016, *MNRAS*, 458, 2371
 Rusli, S. P., Thomas, J., Saglia, R. P., et al. 2013, *AJ*, 146, 45
 Saglia, R. P., Opitsch, M., Erwin, P., et al. 2016, *ApJ*, 818, 47
 Springel, V. 2005, *MNRAS*, 364, 1105
 Thomas, J., Ma, C.-P., McConnell, N. J., et al. 2016, *Natur*, 532, 340
 Thomas, J., Saglia, R. P., Bender, R., Erwin, P., & Fabricius, M. 2014, *ApJ*, 782, 39
 Tsatsi, A., Macciò, A. V., van de Ven, G., & Moster, B. P. 2015, *ApJL*, 802, L3
 van den Bosch, F. C., & Ogiya, G. 2018, *MNRAS*, 475, 4066
 van der Marel, R. P., & Franx, M. 1993, *ApJ*, 407, 525
 Veale, M., Ma, C.-P., Greene, J. E., et al. 2017, *MNRAS*, 471, 1428
 Wellons, S., Torrey, P., Ma, C.-P., et al. 2015, *MNRAS*, 449, 361